



# THB-splines multi-patch parameterization for multiply-connected planar domains via Template Segmentation

Antonella Falini <sup>a,\*</sup>, Bert Jüttler <sup>b</sup>

<sup>a</sup> INdAM c/o University of Florence, Viale Morgagni 67/A, 50134, Firenze, Italy

<sup>b</sup> Institute of Applied Geometry, Johannes Kepler University of Linz, Altenberger Strasse 69, 4040 Linz, Austria

## ARTICLE INFO

### Article history:

Received 16 March 2018

Received in revised form 2 August 2018

### Keywords:

Multi-patch

Parameterization

Isogeometric analysis

Segmentation

THB-splines

## ABSTRACT

Given a planar multiply-connected domain  $\Omega$ , we provide a multi-patch parameterization exploiting a segmentation algorithm and the construction of *templates*. The segmentation is a fundamental step which allows to split the input domain into patches topologically equivalent to quadrilaterals. Templates are prototypes of segmentation that will be chosen according to the shape of the given domain. We will compute a bijective harmonic mapping  $\mathbf{h}$  defined between the input  $\Omega$  and the chosen template  $\hat{\Omega}$ . The segmentation will be transferred from the prototype template to the input  $\Omega$  by approximating the inverse mapping. Templates are equipped with a multi-patch structure and each patch  $\hat{\Omega}^{(i)}$  is parametrized individually by a geometry mapping  $\mathbf{G}_i$ . The final multi-patch parameterization of  $\Omega$  is achieved exploiting the combination of each geometry mapping  $\mathbf{G}_i$  and the inverse of the mapping  $\mathbf{h}$  obtained by projection into the THB-spline space.

© 2018 Elsevier B.V. All rights reserved.

## 1. Introduction

Isogeometric analysis (IgA), introduced in 2005 by T. Hughes et al. in [1], is a new technique used in order to numerically solve differential problems and based on the isoparametric concept; namely, it uses the same shape functions for both, the solution space of the problem unknowns and for the description of the geometric model. In fact, most of the advantages of IgA derive from the use of special spline functions, like NURBS or B-splines, which are the standard technology in CAD modeling. CAD models are usually given through their Boundary Representation (B-Rep), i.e., the solid object is described by the shape of its surfaces and edge curves (see for instance [2]), but in order to perform numerical simulation, a parameterization of the volume is needed. One way to address this problem is to provide *segmentation* techniques which aim at decomposing the given geometric model into several “pieces”, called *patches*, and providing parameterization methods for single or *multi-patch* geometries.

### 1.1. Isogeometric segmentation and parameterization

In order to obtain a multi-patch parameterization of the considered object, we provide an algorithmic procedure to produce a segmentation into topological quadrilaterals, of multiply-connected planar shapes. Therefore, throughout this

\* Corresponding author.

E-mail addresses: [antonella.falini@unisi.it](mailto:antonella.falini@unisi.it) (A. Falini), [bert.juettler@jku.at](mailto:bert.juettler@jku.at) (B. Jüttler).

work, the *isogeometric segmentation* concept refers to the following process: a relatively complex geometric model in 2D, given by its B-Rep, is segmented into several patches topologically equivalent to quadrilaterals.

More precisely, the segmentation leads to a collection of quadrilateral patches  $\Omega^{(i)}$  such that the input domain  $\Omega \subset \mathbb{R}^2$  can be seen as their union,

$$\Omega = \bigcup_{i=0}^{n-1} \Omega^{(i)}. \quad (1)$$

Given an input planar multiply-connected domain we aim at applying a prototype of segmentation to it, and at getting it segmented accordingly. More in detail, we are going to define and construct prototypes of segmentation. Then, in order to apply the chosen segmentation to the input domain  $\Omega$ , we construct an invertible harmonic map between  $\Omega$  and the chosen prototype.

Our algorithm consists of the following main steps:

- (1) Approximation of a bijective harmonic mapping  $\mathbf{h}$  between the input domain  $\Omega$  and an auxiliary domain  $\hat{\Omega}$  via an isogeometric boundary element method.
- (2) Definition of prototypes of segmentations on the auxiliary domain  $\hat{\Omega}$  to get *templates*.
- (3) Approximation of the inverse of  $\mathbf{h}$  to transfer the segmentation to the input  $\Omega$  from the chosen template.

Once the input domain has been decomposed into several patches, each of them can be individually parametrized by a geometric map  $\mathbf{q}^{(i)}$ , defined over the unit square  $[0, 1]^2$  and expressed in terms of tensor-product spline functions as

$$\mathbf{q}^{(i)}(u, v) = \sum_{j \in J} \mathbf{c}_j^{(i)} N_j^{(i)}(u, v), \quad (2)$$

where  $J$  is the set of indices for the considered degrees of freedom,  $\mathbf{c}_j^{(i)} \in \mathbb{R}^2$  are the control points,  $N_j^{(i)}(u, v)$  are the basis functions spanning the space of tensor product splines of a certain degree  $d$  (in our case we always considered  $d = 2$ ) and the index  $i$  refers to the  $i$ th patch in  $\Omega$ .

The geometric map  $\mathbf{q}^{(i)}$  must satisfy some important properties. It is essential to have an injective map, as we need a parameterization free from self-intersections. It is also desirable to obtain iso-parametric elements as uniform as possible and to have an iso-parametric structure as orthogonal as possible. The first requirement will be addressed constructing a bijective harmonic mapping. The last two properties will be recovered using a specific uniformity functional that will improve the quality of the final parameterization.

### 1.2. State of the art

The segmentation process has been investigated and explored in several situations. From isogeometric point of view, the segmentation pipeline has been studied for simply connected solids without non-convex edges in [3,4], and for general three-dimensional solids, segmented into simply connected ones in [5].

Several approaches have been investigated in IgA in order to construct good parameterizations. For instance, Coons patches, described in [6], are a simple technique, but the resulting map may not be injective and is not suitable for singular cases or complex shapes. An improvement is achieved by the spring model (cf. [7]), that although is slightly more expensive, provides a better quality parameterization. Other methods based on the mean-value coordinates are also investigated in [8] and more generally, various techniques for mesh and surface parameterization can be found in [9,10] and references cited therein.

A method based on domain decompositions achieved via skeleton computation is proposed in [11]. A patch-adjacency graph technique which identifies the optimal multi-patch parameterization with respect to an objective function that captures the parameterization quality has been introduced in [12]. In order to achieve a more uniform parameterization, a method based on the specific quasi-conformal Teichmüller map is proposed in [13]. In [14] the authors propose a method to segment in quads planar domains with high genus and construct an IgA-suitable parameterization of the input.

Also, in order to perform adaptive numerical simulation there is the need to use basis functions which allow for local refinement. Some examples of parameterizations obtained with “non-standard” B-splines are: [15] where T-splines are used, [16] with Powell–Sabin splines based parameterizations, [17] where THB-splines are employed.

### 1.3. Outline

The remainder of the paper is structured as follows. In Section 2 we review some fundamental results about harmonic mappings. In particular the presented theorem provides a theoretical framework to the existence of a bijective harmonic mapping between any multiply-connected domain and the punctured unit disk.

In Section 3 we present the boundary element method as an effective method to compute harmonic mappings. The existence of a bijective harmonic mapping requires to provide the location of punctures (pinch points), suitably removed from the unit disk. In fact, freely choosing the location of those points may lead to not bijective mappings; therefore,

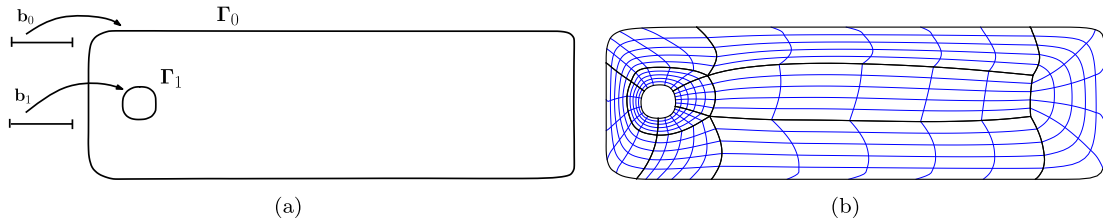


**Fig. 1.** (a) A doubly connected domain  $\Omega$  with boundary curves  $\Gamma_0$  and  $\Gamma_1$ , expressed using the 1-periodic parameterizations  $\mathbf{b}_0, \mathbf{b}_1$ . (b) A multipatch parameterization of the domain  $\Omega$  obtained using THB-splines (see Section 7).

providing a suitable location is of fundamental importance. In Section 4 an optimization problem will be formulated in order to achieve this goal.

Section 5 explains the construction of templates. A template is constructed by segmenting the unit disk into patches, topologically equivalent to quadrilaterals. This segmentation is then transferred to the input domain using the inverse of the harmonic mapping. Results of the segmentation algorithm are presented in Section 6 where also some examples of parameterizations obtained with THB-splines are shown. In Section 7 we explain how to construct a multi-patch parameterization for a multiply-connected planar input suitably segmented.

## 2. Theoretical foundation

### 2.1. Problem formulation

The purpose of this study consists in finding a multi-patch parameterization of a multiply-connected planar domain which is given in terms of its boundary components.

We define some notation. Let  $\Omega \subset \mathbb{R}^2$  be the input planar domain, which consists of simply closed curves  $\Gamma_i$  such that  $\bigcup_{i=0}^n \Gamma_i$  is the boundary  $\partial\Omega$ . We introduce a 1-periodic parameterization  $\mathbf{b}_i(u)$ ,  $u \in \mathbb{R}$  for each boundary curve  $\Gamma_i$  (see Fig. 1a). We propose an algorithmic procedure which aims at splitting  $\Omega$  into patches topologically equivalent to quadrilaterals such that we can construct a multi-patch parameterization of the input domain (see Fig. 1b).

### 2.2. Harmonic mapping to auxiliary domain: punctured disk

Given a multiply-connected planar domain  $\Omega$ , we introduce an auxiliary domain  $\hat{\Omega}$ , such that its topology matches the one of  $\Omega$ . We look for a bijective map  $\mathbf{h}$ , such that  $\mathbf{h} : \Omega \rightarrow \hat{\Omega}$ .

For the simply connected case, the Riemann mapping theorem and the Radó – Kneser–Choquet theorem provide a theoretical framework for the construction of a univalent harmonic mapping, see [17] for the details. In particular, the Radó – Kneser–Choquet theorem asserts that the unit disk can always be harmonically mapped onto a convex domain, bounded by a Jordan curve, provided a homeomorphic boundary correspondence.

In Duren and Hengartner [18] the authors prove an extension to the Radó – Kneser–Choquet theorem for the multiply-connected case. We report the statement of the theorem using our notation.

**Theorem 1** (Duren–Hengartner). *Let  $\Omega \subset \mathbb{R}^2$  be a multiply-connected domain bounded by Jordan curves  $\Gamma_0, \Gamma_1, \dots, \Gamma_n$ , where  $\Gamma_0$  is the outer boundary component. Let  $\tilde{\Omega} \subset \mathbb{R}^2$  be a bounded convex domain and let  $\mathbf{f}_0$  be an orientation-preserving continuous and monotone map of  $\Gamma_0$  onto  $\partial\tilde{\Omega}$ . Then there exists a function  $\mathbf{h}$  harmonic in  $\Omega$  and continuous in  $\bar{\Omega}$ , which maps  $\Omega$  univalently (i.e., one to one) onto  $\tilde{\Omega}$  with  $n$  points removed and with the prescribed boundary values:  $\mathbf{h}(z) = \mathbf{f}_0(z)$  on  $\Gamma_0$ .*

According to the specifics required by Theorem 1, we define our auxiliary domain  $\hat{\Omega} := \tilde{\Omega} \setminus \{\hat{\mathbf{p}}_1 \dots \hat{\mathbf{p}}_n\}$ , where the set  $\{\hat{\mathbf{p}}_1 \dots \hat{\mathbf{p}}_n\}$  denotes  $n$ -points removed from the inside of  $\tilde{\Omega}$ . Using Theorem 1 and the fact that, by definition, harmonic functions solve the Laplace equation, we can formulate the following Dirichlet problem: Find  $\mathbf{h}$  such that

$$\begin{cases} \Delta \mathbf{h} = 0 & \text{in } \Omega, \\ \mathbf{h}(\mathbf{x}) = \mathbf{f}_0(\mathbf{x}) & \text{on } \Gamma_0, \\ \mathbf{h}(\mathbf{x}) = \hat{\mathbf{p}}_i & \text{on } \Gamma_i, \quad i = 1, \dots, n. \end{cases} \quad (3)$$

where  $\mathbf{f}_0 : \Gamma_0 \rightarrow \partial\hat{\Omega}$  is the given boundary correspondence,  $\hat{\mathbf{p}}_i$  are the punctures in  $\hat{\Omega}$ ,  $\Gamma_0$  and  $\Gamma_i$ ,  $i = 1, \dots, n$  as in Theorem 1. We choose  $\Omega$  as a planar domain, therefore, the map  $\mathbf{h}$  will consist of two components  $\mathbf{h} = (h_1, h_2)$ . Hence, we are going to solve the Laplace problem (3) twice (once for each component).

The computation of the map  $\mathbf{h}$  is carried out with a boundary element method technique adapted to handle multiply-connected domains. Further details follow in the subsequent section.

### 3. Computing harmonic mappings by isogeometric BEM

The *boundary element method* (BEM) is a numerical method widely used to solve PDEs (cf. [19,20]). The main idea is to reduce the dimension of the problem by one using a *boundary integral equation* (BIE) where the unknown is defined only on the boundary of the computational domain, so that no mesh or parameterization of the interior is needed.

#### 3.1. BIE for the Laplace problem

In order to transform the PDE into an integral equation we need to provide the fundamental solution for the differential operator of the PDE. For the Laplace operator in 2D, the fundamental solution coincides with the Green function

$$\mathcal{G}(\mathbf{x}, \mathbf{y}) = -\frac{1}{2\pi} \ln(|\mathbf{x} - \mathbf{y}|). \quad (4)$$

Then, we can express the solution  $\mathbf{h}$  of (3) through the *representation formula* (5), in terms of Dirichlet data  $\mathbf{h}_{D_i} = \mathbf{h}|_{\Gamma_i}$  and Neumann data  $\mathbf{h}_{N_i} = \frac{\partial \mathbf{h}}{\partial \mathbf{n}}|_{\Gamma_i}$

$$\alpha \mathbf{h}(\mathbf{y}) = \sum_{i=0}^n \left[ \int_{\Gamma_i} \mathcal{G}(\mathbf{x}, \mathbf{y}) \mathbf{h}_{N_i} d\Gamma_i - \int_{\Gamma_i} \mathbf{h}_{D_i}(\mathbf{x}) \frac{\partial \mathcal{G}(\mathbf{x}, \mathbf{y})}{\partial \mathbf{n}} d\Gamma_i \right] \quad (5)$$

where

$$\alpha = \begin{cases} 1 & \text{if } \mathbf{y} \in \Omega, \\ \frac{1}{2} & \text{if } \mathbf{y} \in \partial\Omega, \\ 0 & \text{otherwise,} \end{cases}$$

and  $\frac{\partial \mathcal{G}(\mathbf{x}, \mathbf{y})}{\partial \mathbf{n}}$  is the normal derivative of  $\mathcal{G}$  with respect to the first argument, i.e.,

$$\frac{\partial \mathcal{G}(\mathbf{x}, \mathbf{y})}{\partial \mathbf{n}} = \frac{d}{d\tau} \mathcal{G}(\mathbf{x} + \tau \mathbf{n}_x, \mathbf{y})|_{\tau=0}.$$

If both, the Dirichlet data and the Neumann data, are known Eq. (5) can be applied with  $\alpha = 1$ , in order to evaluate  $\mathbf{h}$  at any point in the interior of  $\Omega$ . Otherwise, if one of the boundary data is missing, the representation formula can be used as a BIE in order to compute the unknown value.

In our case we solve a BIE for the unknown flux  $\mathbf{h}_N$ , with  $\alpha = 1/2$  and  $\mathbf{y} \in \partial\Omega$ .

We introduce the following notation:

- We denote by  $\mathbf{f}_0$  the boundary correspondence of problem (3) such that  $\mathbf{h}_{D_0} = \mathbf{h}|_{\Gamma_0} = \mathbf{f}_0 : \Gamma_0 \rightarrow \partial\hat{\Omega}$ ,
- The given punctures  $\hat{\mathbf{p}}_i$  are expressed through functions  $\{\mathbf{f}_i\}_{i=1}^n$  such that  $\mathbf{h}_{D_i} = \mathbf{h}|_{\Gamma_i} = \mathbf{f}_i : \Gamma_i \rightarrow \hat{\mathbf{p}}_i$ ,
- The flux of the solution  $\mathbf{h}$  relative to the boundary component  $\Gamma_i$  is denoted by  $\mathbf{g}_i = \mathbf{h}_{N_i}$ .

For a given multiply-connected domain  $\Omega$ , with boundary curves  $\{\Gamma_i\}_{i=0}^n$ , we derive the following BIE,

$$\frac{1}{2} \mathbf{f}_\ell(\mathbf{y}) = \sum_{i=0}^n \left[ \int_{\Gamma_i} \mathcal{G}(\mathbf{x}, \mathbf{y}) \mathbf{g}_i(\mathbf{x}) d\Gamma_i - \int_{\Gamma_i} \mathbf{f}_i(\mathbf{x}) \frac{\partial \mathcal{G}(\mathbf{x}, \mathbf{y})}{\partial \mathbf{n}} d\Gamma_i \right] \quad \forall \mathbf{y} \in \Gamma_\ell, \forall \ell = 0, \dots, n. \quad (6)$$

The outer boundary  $\Gamma_0$  is counterclockwise oriented, therefore, the normal vector  $\mathbf{n}$  is outward pointing. For  $i = 1, \dots, n$ , each  $\Gamma_i$  is clockwise oriented, hence  $\mathbf{n}$  is inward pointing.

#### 3.2. Isogeometric discretization

As described in Section 2.1, the input domain  $\Omega$  is given in terms of its boundary components  $\{\Gamma_i\}_{i=0}^n$ , that are expressed through 1-periodic parameterizations  $\mathbf{b}_i(u)$ ,  $u \in \mathbb{R}$ . Consequently, we can express:

- The flux of  $\mathbf{h}$  in terms of  $\mathbf{b}_i$ ,  $i = 0, \dots, n$ :

$$\hat{\mathbf{g}}_i(u) = \mathbf{g}_i \circ \mathbf{b}_i(u).$$

- Each boundary function  $\mathbf{f}_i$  as:

$$\hat{\mathbf{f}}_i(u) = \mathbf{f}_i \circ \mathbf{b}_i(u) \quad \forall i = 0, \dots, n.$$

We can now transform the integrals of Eq. (6) to the unit interval  $[0, 1]$ :

$$\frac{1}{2}\hat{\mathbf{f}}_\ell(v) = \sum_{i=0}^n \left[ \int_0^1 \mathcal{G}(\mathbf{b}_i(u), \mathbf{b}_\ell(v)) \hat{\mathbf{g}}_i(u) \|\dot{\mathbf{b}}_i(u)\| du - \int_0^1 \hat{\mathbf{f}}_i(u) \frac{\partial \mathcal{G}(\mathbf{b}_i(u), \mathbf{b}_\ell(v))}{\partial \mathbf{n}} \|\dot{\mathbf{b}}_i(u)\| du \right] \quad \forall \ell, \forall v. \quad (7)$$

Eq. (7) needs to be discretized and then solved for the unknown flux  $\hat{\mathbf{g}}_i$  which will be expressed in terms of spline functions  $N_{i,j}$  and unknown control points  $\mathbf{c}_{i,j}$  (the subscript  $i$  refers to the  $i$ th boundary component) as,

$$\hat{\mathbf{g}}_i(u) = \sum_{j=1}^{m_i} \mathbf{c}_{i,j} N_{i,j}(u), \quad u \in [0, 1]. \quad (8)$$

The unknowns  $\mathbf{c}_{i,j}$  can be computed by the collocation method (see for instance [21]), i.e. by requiring Eq. (7) to hold at specific values that we choose to be the Greville abscissas  $(v_k^\ell)$ ,  $k = 0, \dots, m_\ell$ ,  $\ell = 0, \dots, n$ .

$$\frac{1}{2}\hat{\mathbf{f}}_\ell(v_k^\ell) = \sum_{i=0}^n \left[ \int_0^1 \mathcal{G}(\mathbf{b}_i(u), \mathbf{b}_\ell(v_k^\ell)) \sum_{j=1}^{m_i} \mathbf{c}_{i,j} N_{i,j}(u) \|\dot{\mathbf{b}}_i(u)\| du - \int_0^1 \hat{\mathbf{f}}_i(u) \frac{\partial \mathcal{G}(\mathbf{b}_i(u), \mathbf{b}_\ell(v_k^\ell))}{\partial \mathbf{n}} \|\dot{\mathbf{b}}_i(u)\| du \right] \quad \forall \ell, \forall k. \quad (9)$$

We can rearrange Eq. (9) as follows:

$$\sum_{i=0}^n \sum_{j=0}^{m_i} \mathbf{c}_{i,j} \int_0^1 \mathcal{G}(\mathbf{b}_i(u), \mathbf{b}_\ell(v_k^\ell)) N_{i,j}(u) \|\dot{\mathbf{b}}_i(u)\| du = \frac{1}{2}\hat{\mathbf{f}}_\ell(v_k^\ell) + \sum_{i=0}^n \int_0^1 \hat{\mathbf{f}}_i(u) \frac{\partial \mathcal{G}(\mathbf{b}_i(u), \mathbf{b}_\ell(v_k^\ell))}{\partial \mathbf{n}} \|\dot{\mathbf{b}}_i(u)\| du \quad \forall \ell, \forall k. \quad (10)$$

More precisely, we arrive at a linear system  $\mathbf{A}\mathbf{c} = \mathbf{B}$ , with the matrix  $\mathbf{A} = (a_{(l,k)(i,j)})$  and right hand side  $\mathbf{B} = (b_{(l,k)i})$ . The entries of the matrix are given by the term on the left hand side of Eq. (10):

$$a_{(l,k)(i,j)} = \int_0^1 \mathcal{G}(\mathbf{b}_i(u), \mathbf{b}_\ell(v_k^\ell)) N_{i,j}(u) \|\dot{\mathbf{b}}_i(u)\| du.$$

The unknowns are the control points  $\mathbf{c}_{i,j}$  and the entries of the vector  $\mathbf{B}$  are:

$$b_{(l,k)i} = \frac{1}{2}\hat{\mathbf{f}}_\ell(v_k^\ell) + \int_0^1 \hat{\mathbf{f}}_i(u) \frac{\partial \mathcal{G}(\mathbf{b}_i(u), \mathbf{b}_\ell(v_k^\ell))}{\partial \mathbf{n}} \|\dot{\mathbf{b}}_i(u)\| du.$$

The solution of the linear system allows us to compute the flux  $\mathbf{h}_\mathbf{n}$ . Then, using the representation formula (5) with  $\alpha = 1$ , we can evaluate the map  $\mathbf{h}$  at any point  $\mathbf{y}$  in  $\Omega$ .

One of the main issue about BEM regards the evaluation of singular integrals. From the definition of the Green function  $\mathcal{G}$  (Eq. (4)), it is clear that as the integration point  $\mathbf{x}$  approaches the collocation point  $\mathbf{y}$ , the value of  $\mathcal{G}$  and the value of its normal derivative get indeterminate and the integrals in Eq. (10) become singular. In order to tackle this problem several techniques have been developed such as, singularity subtraction schemes [22], generalized Gaussian quadrature [23], singular weighted quadrature rules [24,25] or even a combination of those techniques used together in order to improve efficiency and accuracy.

#### 4. Punctures determination

The hypothesis expressed in Theorem 1 requires to remove suitably placed punctures from the auxiliary domain  $\hat{\Omega}$ . Indeed, freely choosing the location of the Dirichlet boundary conditions  $\hat{\mathbf{P}}_i$  may lead to not injective harmonic mappings as it is shown in the following example. Let us consider the doubly connected domain of Fig. 1a with the auxiliary domain  $\hat{\Omega}$  depicted in Fig. 2c. We solve the Laplace problem (11), imposing the Dirichlet condition on the boundary  $\Gamma_1$  equal to the point  $\hat{\mathbf{P}}_1 = (-0.1, -0.1)$ :

$$\begin{cases} \Delta \mathbf{h} = 0 & \text{in } \Omega, \\ \mathbf{h}(\mathbf{x}) = \mathbf{f}_0(\mathbf{x}) & \text{on } \Gamma_0, \\ \mathbf{h}(\mathbf{x}) = \hat{\mathbf{P}}_1 & \text{on } \Gamma_1. \end{cases} \quad (11)$$

In order to display the harmonic mapping  $\mathbf{h}$  solution of the problem (11), we generate a grid mesh inside the input domain  $\Omega$  Fig. 2a, and we map this structure to  $\hat{\Omega}$ , Fig. 2b. We notice the occurrence of overlappings and foldings in a neighborhood of the point  $\hat{\mathbf{P}}_1$  (see Fig. 2b) which implies a not bijective mapping  $\mathbf{h}$ . Therefore, providing suitably located  $\hat{\mathbf{P}}_i$  is essential to guarantee injectivity. To this end, we formulate an optimization problem, noticing that the presence of overlappings and foldings increases the computed value for the area of  $\hat{\Omega}$ , through the parameterization provided by  $\mathbf{h}$ . Therefore, one possible way to find an injective map is to try to minimize the value of the parametrized area  $A(\hat{\mathbf{P}})$  of  $\hat{\Omega}$ , where with  $\hat{\mathbf{P}}$  we denote the set of  $\hat{\mathbf{P}}_i$ .

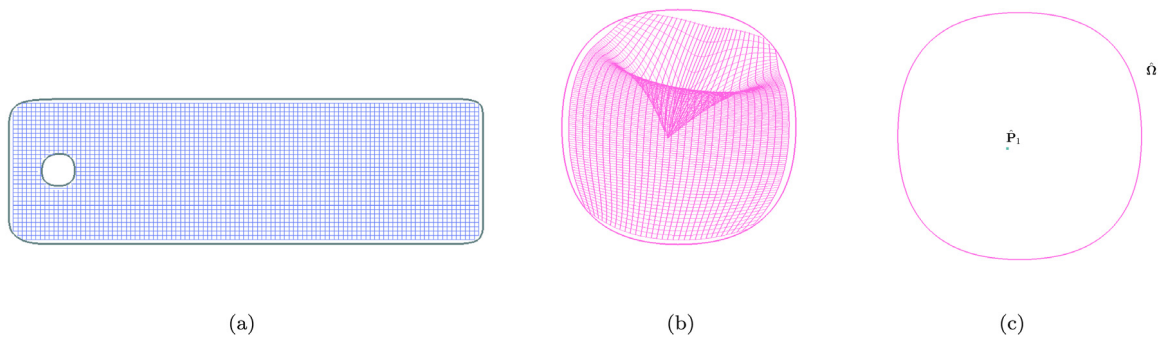


**Fig. 2.** (a) A grid mesh is generated inside  $\Omega$ . (b) The image of the mesh through the map  $\mathbf{h}$  shows overlappings and foldings in the neighborhood of the point  $\hat{\mathbf{P}}_1$ . (c) The auxiliary domain  $\hat{\Omega}$  is chosen as a B-spline approximation of the unit circle with one point  $\hat{\mathbf{P}}_1 = (-0.1, -0.1)$  removed. The location of  $\hat{\mathbf{P}}_1$  is arbitrarily chosen.

#### 4.1. Formulation of an optimization problem

We formulate the following optimization problem,

$$\text{Find } \hat{\mathbf{P}} \in \hat{\Omega} \text{ such that } A(\hat{\mathbf{P}}) \text{ is minimal.} \quad (12)$$

The objective function is defined as:

$$A(\hat{\mathbf{P}}) := \int_{\Omega} |\det J_{\mathbf{h}}| d\Omega \quad (13)$$

where  $J_{\mathbf{h}}$  is the Jacobian matrix of the harmonic mapping  $\mathbf{h}$ , therefore,  $A(\hat{\mathbf{P}})$  will be the computed area through the parameterization provided by  $\mathbf{h}$ . The minimization problem (12) can now be stated as follows:

$$\text{Find } \hat{\mathbf{P}} \in \hat{\Omega} \text{ such that } \hat{\mathbf{P}} = \arg \min A. \quad (14)$$

If the input domain  $\Omega$  has connectivity  $n + 1$ , we need to find the location of  $n$  points  $\hat{\mathbf{P}}_i$  in  $\hat{\Omega}$  solving a minimization problem with  $2n$  unknowns, where  $n$  is the number of holes in  $\Omega$ .

We choose to find the minimum of  $A$  using a derivative-free method [26,27]. This kind of strategy tries to provide a set of good directions (i.e. directions where the objective function decreases its value) and it operates using also a line-search technique, which can increase the convergence speed, providing a big step once a good direction has been detected. We adopted the third algorithm proposed in [27], modifying the stop criterion as follows.

Firstly, we computed the area of the auxiliary domain  $\hat{\Omega}$  using the following:

Given a parameterization  $\mathbf{r} = (x(t), y(t))$   $t \in [a, b]$  of  $\partial\hat{\Omega}$ , the area  $\hat{A}$  bounded by the curve spanned by  $\mathbf{r}$  can be computed by:

$$\hat{A} = - \int_a^b y(t) \dot{x}(t) dt. \quad (15)$$

Secondly, the value of  $\hat{A}$  is chosen as optimal minimum. Nevertheless, reaching this value cannot be adopted as a stop criterion. In fact, the grid structure generated in  $\Omega$  is not perfectly covering the inside of the considered domain. As a consequence, the grid obtained in  $\hat{\Omega}$ , in practice, covers a smaller area than the effective one. Therefore, the chosen derivative-free algorithm is iterated until the value of  $A(\hat{\mathbf{P}})$  is less than  $\hat{A}$ . We also approximate the integral in (13) through a Riemann sum. Although more advanced techniques exist in order to tackle this computation (see for example [28,29]), in our case the numerical approximation of the integral (13) provided a sufficiently accurate solution.

Solving (12)–(13) will optimize the location of the punctures in  $\hat{\mathbf{P}}$  in such a way to produce an area  $A(\hat{\mathbf{P}})$  which is as close as possible to the optimal value  $\hat{A}$ . Unfortunately local minima cannot be avoided by the proposed technique. If the algorithm gets stuck in a local minimum, the process is restarted with a different initial configuration.

We verified that for all the proposed examples the resulting  $\hat{\mathbf{P}}$  provides an orientation preserving mapping  $\mathbf{h}$ , where folding and overlapping result removed.

#### 4.2. Example

The Fig. 3a shows the resulting mapping  $\mathbf{h}$ , with Dirichlet condition on  $\Gamma_1$  given by the solution of the optimization problem (14). The optimization history can be found in Table 1 and the path of the point  $\hat{\mathbf{P}}_1$  is shown in Fig. 3b.

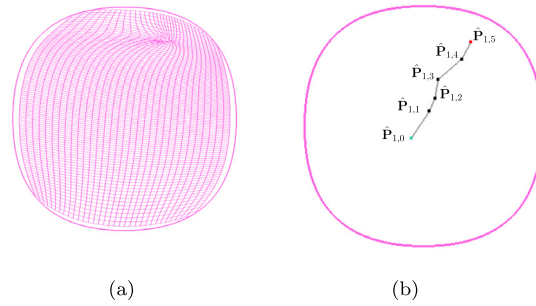


**Fig. 3.** (a) The solution of the optimization problem (14) provides the location of the puncture  $\hat{\mathbf{P}}_1$  such that the computed mapping  $\mathbf{h}$  is injective. (b) The picture shows the path of the point  $\hat{\mathbf{P}}_1$  according to the data of Table 1.

**Table 1**

Steps of the optimization algorithm for the example shown in Fig. 3, with  $K$  iterations starting from the point  $\hat{\mathbf{P}}_{1,0} = (-0.1, -0.1)$ .

$K$	0	1	2	3	4	5
$\hat{\mathbf{P}}_{1,K}$	$(-0.1, -0.1)$	$(0.05, 0.123)$	$(0.0987, 0.235)$	$(0.125, 0.389)$	$(0.3245, 0.56)$	$(0.4, 0.7)$
$A(\hat{\mathbf{P}})$	3.78	3.65	3.49	3.37	3.34	3.28

## 5. Template selection

In this section we describe how to construct a *template* according to the shape of the input domain  $\Omega$ . More precisely, the chosen auxiliary domain  $\hat{\Omega}$  must match the topology of  $\Omega$  and hence, it will have as many punctures as the number of holes of  $\Omega$ . Additionally, it will be equipped with a segmentation first, and then with a multi-patch structure. These last two steps will lead to the define a *prototype* that we will refer to as *template*.

Also, we require extraordinary vertices (EVs) in order to achieve a quadrilateral segmentation in the input domain and we distinguish between EVs on the boundary and EVs in the interior.

The templates are collected in an (incomplete) catalog, and they are classified by the number of punctures (singular points) and valencies ( $\mu_j$ ) of the inner EVs. More in detail, to any configuration is associated a *deficit*  $d$  (see for instance [30]) computed as:

$$d = \sum_{j=1}^{\text{inner vertices}} (\mu_j - 4).$$

The deficit is used to construct different templates for any case (2-connected, 3-connected, 4-connected case, and so on). The catalog could be preliminarily generated, and even though it is not exhaustive, any segmentation for a specific case is identified by the same deficit. Hence, once the location of the punctures has been identified, one can choose a specific item from the catalog. The segmentation structure changes according to the location of the punctures. Nevertheless, we can still provide some general guidelines:

- Identification of the punctures  $\hat{\mathbf{P}}_i$ ,  $i = 1, \dots, n$ ,
- Construction of circles centered at the punctures,
- Star-connections between the punctures and the circles,
- Creation of inner EVs with different valencies,
- Connections with the outer boundary  $\partial\hat{\Omega}$ .

In the following example we present two possible templates (Fig. 4a and c) for the doubly connected case. The deficit associated to any of these configurations is  $d = 0$ . The template in Fig. 4a is more suitable if the input domain  $\Omega$  possesses one hole located in a rather central position; while the template in Fig. 4c is recommended when the hole is located close to the boundary. The resulting segmentations in  $\Omega$ , shown in Fig. 4b and d, highlight how the template (c) can handle better the shape of the input domain.

## 6. Segmentation results

In this section we present some examples of segmentation for multiply-connected domains. The choice of the right template is strongly dependent on the shape of the input domain, as every suggested segmentation produces a different output on  $\Omega$ .

Additionally, we can classify a segmentation on the base of its complexity. In general the simplest segmentations have only EVs with valency 5, as they create nice quadrilaterals, and do not involve many splitting curves inside  $\hat{\Omega}$ . The



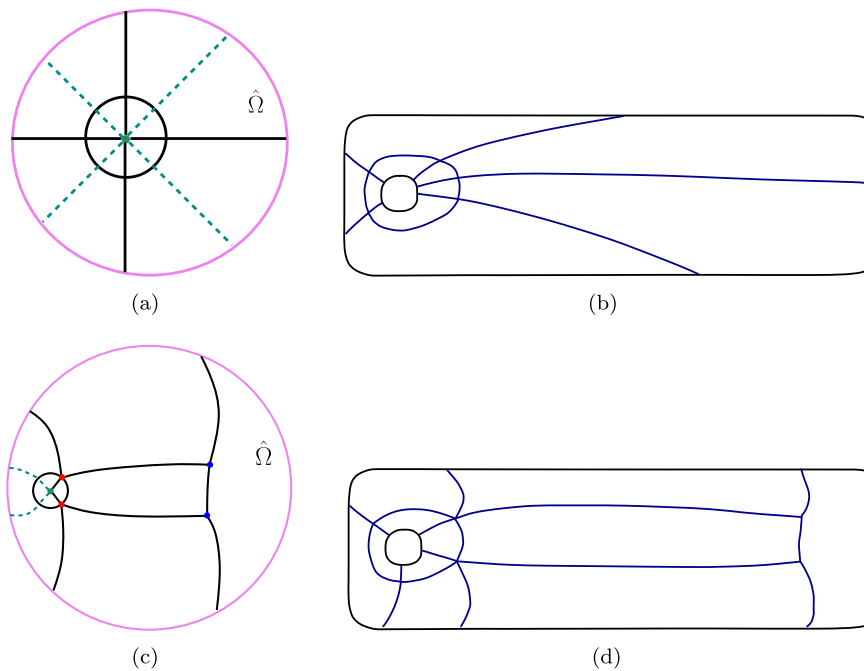


**Fig. 4.** (a) The template  $\hat{\Omega}$  has the simplest structure with no EVs. The dashed curves represent optional splitting. (b) The domain  $\Omega$  is segmented according to the template (a) where we also used some additional optional splitting to improve the final segmentation. (c) This segmentation is achieved using two EVs with valency 5 in red and two EVs with valency 3 in blue. (d) The input  $\Omega$  segmented according to template (c). (For interpretation of the references to color in this figure legend, the reader is referred to the web version of this article.)

segmentations which use also EVs with valency 6 have medium complexity, whereas the segmentations with EVs of valency 3 are classified as the most complex ones, as the presence of such EVs creates distorted quadrilaterals and increases a lot the number of the final patches.

**Example 1.** In this example we present a 3-connected domain  $\Omega$  depicted in Fig. 5a. In Fig. 5b we see the behavior of the harmonic mapping  $\mathbf{h}$ , with Dirichlet boundary conditions provided by the solution of the optimization problem (12).

In Fig. 5c and f we present two possible templates for the 3-connected case. The associated deficit is  $d = 4$ . The pictures 5d and 5g show the input  $\Omega$  segmented according to the aforementioned templates. In this case, both templates provide a reasonable segmentation. The choice of one segmentation rather than the other one, besides depending on the shape of the input domain, is at the user's discretion. For instance, the segmentation shown in Fig. 5d is rather simple and provides 16 quadrilateral patches. The segmentation shown in Fig. 5g, although is rather complex (i.e., it consists of 25 patches and EVs with valency 7 and 3), is able to provide more splitting in the upper region of  $\Omega$ .

In Fig. 5e we also show a multi-patch parameterization of  $\Omega$  previously segmented as in Fig. 5d. The parameterization is obtained using THB-splines. We display the hierarchical meshes for the patches 0, 10, 12 over the parameter domain in Fig. 6.

**Example 2.** The input domain  $\Omega$  is 4-connected (see Fig. 7a). The Dirichlet boundary conditions for the problem (3) are computed solving the optimization problem (12) and the behavior of the resulting harmonic mapping  $\mathbf{h}$  is shown in Fig. 7b. The suggested templates for this case are shown in Fig. 7c and f. The computed deficit is  $d = 8$ . This example remarks the importance of choosing the right template: the segmentation shown in Fig. 7g presents very distorted quads, therefore is very far from being a suitable one, whereas the segmentation obtained in Fig. 7d provides nice quadrilaterals. A multi-patch parameterization of the input  $\Omega$  is shown in Fig. 7e. In Fig. 8 we show the hierarchical meshes for patches 0, 3, 5.

## 7. Multi-patch parameterization

This section is devoted to explain how to achieve a *multi-patch parameterization* for any multiply-connected planar domain, provided a suitable segmentation of it.

First of all it is required to create a multi-patch structure of the template geometry (Section 7.1). Subsequently, we can use the inverse mapping  $\mathbf{h}^{-1}$  and a least-squares fitting technique to solve a suitable minimization problem (Section 7.2). Finally, we perform adaptive refinement using truncated hierarchical B-splines (THB-splines) in order to obtain the desired parameterization of the given input domain  $\Omega$ .



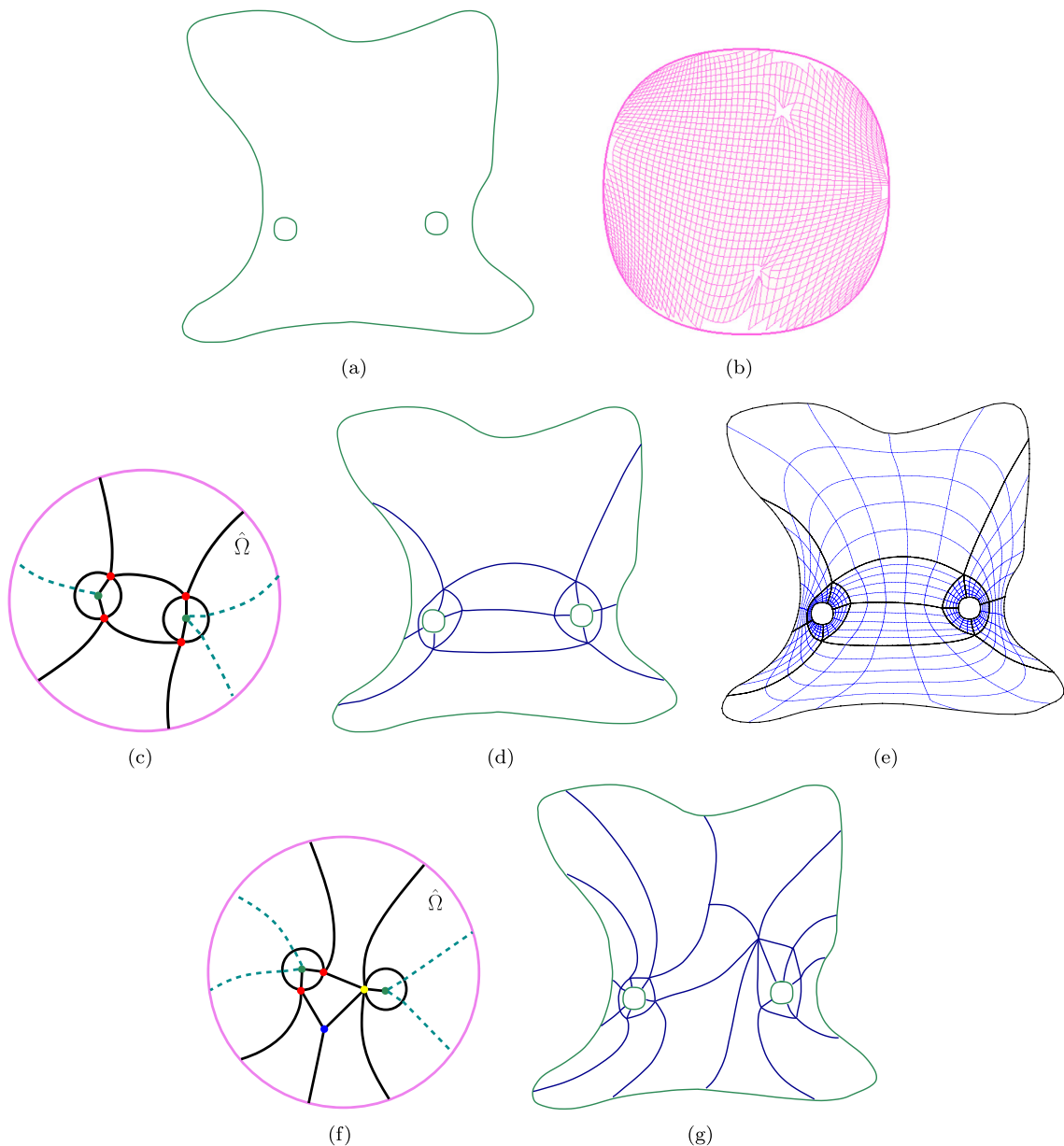


**Fig. 5.** (a) A 3-connected domain  $\Omega$ . (b) The result of the optimization problem (12). In this case the algorithm provides the location of two punctures. The picture shows the behavior of the harmonic mapping  $\mathbf{h}$ , computed by BEM. (c) One possible template for the 3-connected case. The suggested segmentation is obtained exploiting EVs of valency 5 (red spots). (d) The input domain  $\Omega$  is suitably segmented with the template c. (e) The domain  $\Omega$  is parametrized with THB-splines. (f) A second possible template for the 3-connected case. The EVs with valency 3 (blue spot), 5 (red spots) and 7 (yellow spot) are highlighted. (g) The domain  $\Omega$  segmented according to template f. (For interpretation of the references to color in this figure legend, the reader is referred to the web version of this article.)

### 7.1. Template creation: last step

Once the most suitable template has been chosen from the catalog, we create a multi-patch structure using Gordon–Coons technique (cf. [6]), where singular patches happen in the vicinity of the punctures. The curves defining the segmentation of the template are quadratic B-spline functions. They are constructed in such a way that the number of control points and the number of knots are equal for each of them.

The outer boundary of  $\hat{\Omega}$  is split at the intersection points with the segmentation curves applying the knot insertion algorithm (see for example [31], Chapter 5). At this point, each patch, regular or singular, is parametrized applying Coons technique. Using this strategy we get a multi-patch parameterization of the template with unit squares as parametric domains. The resulting patches are finally joined with  $C^0$  smoothness.

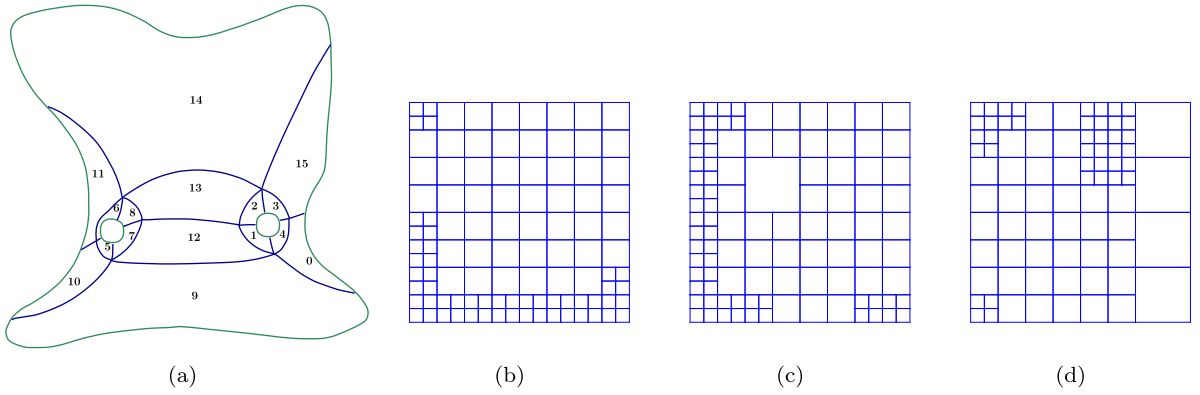


**Fig. 6.** (a) The segmented input  $\Omega$  where each patch is labeled with a number. The multi-patch parameterization shown in Fig. 5e is obtained with 5 adaptive refinement iterations. The hierarchical meshes for the patch 0 (b), patch 10 (c) and patch 12 (d) are displayed over the parameter domains.

## 7.2. A fitting problem

The multi-patch parameterization of the template provides a geometric map  $\mathbf{G}_i$  for each patch  $i$ , defined over the unit square  $[0, 1]^2$ . The solution of the problem (3) with the suitable boundary conditions provides a bijective harmonic mapping  $\mathbf{h} : \Omega \rightarrow \hat{\Omega}$ . We aim at constructing a multi-patch parameterization of the given  $\Omega$  using THB-splines and exploiting the combination of  $\mathbf{h}^{-1}$  with  $\mathbf{G}_i$  for every patch  $\Omega^{(i)}$  (see Fig. 9).

Let  $\mathbf{q}_i$  denote the unknown parameterization of each patch  $\Omega^{(i)}$  of  $\Omega$ , we formulate the following fitting problem,

$$\|\mathbf{q}_i - \mathbf{h}^{-1} \circ \mathbf{G}_i\|_{L^2}^2 \rightarrow \min \quad \forall \text{ patch } \Omega^{(i)} \quad (16)$$

which gives the least-square approximation of  $\mathbf{q}_i$ . Discretizing (16) gives,

$$\sum_i \sum_j (\mathbf{q}_i(u_j, v_j) - \mathbf{h}^{-1} \circ \mathbf{G}_i(u_j, v_j))^2 \rightarrow \min \quad \forall \text{ patch } \Omega^{(i)}. \quad (17)$$

We solve (17) through the following steps:

- (1) We sample points  $(u_j, v_j)$  in  $[0, 1]^2$ ,
- (2) We map the sampling points to the template  $\hat{\Omega}$ , patch-wise, using the corresponding  $\mathbf{G}_i$ ,
- (3) We approximate  $\mathbf{h}^{-1}$ ,
- (4) We use adaptive refinement.

Step (1) and (2) are achieved as follows. The unit square is sampled with uniform grid points. These samples are then mapped through  $\mathbf{G}_i$  to the patch  $i$  of the template. The grid points in the unit square provide parameter values for any fitting technique one wants to adopt in order to solve (16). The physical values used for the fitting are provided evaluating the inverse of  $\mathbf{h}$  at the template's samples.

The process just described is done patch-wise. If the patch in  $\hat{\Omega}$  happens to be a singular one, one of the edges of the corresponding patch in  $\Omega$  will be a part of the boundary curve of the corresponding hole. In this case, the parameter values are obtained sampling the edge of the unit box corresponding to the singular point, but the physical values (in patch  $\Omega^{(i)}$ ) are computed through the orthogonal projection to the boundary curve defining the hole taken into account.

Regarding step (3), the approximation of the inverse mapping  $\mathbf{h}^{-1}$  can be done using a predictor–corrector technique if we are only interested in tracing the segmentation curves, see Section 4 in [32] where this method is referred to as *tracing algorithm*. On the other hand, in order to achieve also a parameterization of the given  $\Omega$ , the inverse mapping  $\mathbf{h}^{-1}$  is projected into the THB-spline space. We refer to [17] for the explanation of the steps involved in this procedure. Finally, about the evaluation of the inverse of  $\mathbf{h}$  on the outer boundary, we exploit the Dirichlet boundary condition expressed as  $\mathbf{f}_0$  in problem (3).

The step (4) highlights the use of the adaptive refinement procedure. In fact, the desired parameterization  $\mathbf{q}_i$  is expressed through THB-splines basis functions as

$$\mathbf{q}_i(u, v) = \sum_{\ell=1}^L \sum_{k=1}^{K^\ell} \mathbf{c}_k^\ell \tau_k^\ell(u, v), \quad (u, v) \in [0, 1]^2, \quad \forall \text{ patch } \Omega^{(i)}, \quad (18)$$

where  $\ell$  identifies the level,  $L$  is the number of all levels in the hierarchy and  $K^\ell$  is the number of THB-splines  $\tau_k^\ell$  at level  $\ell$ .

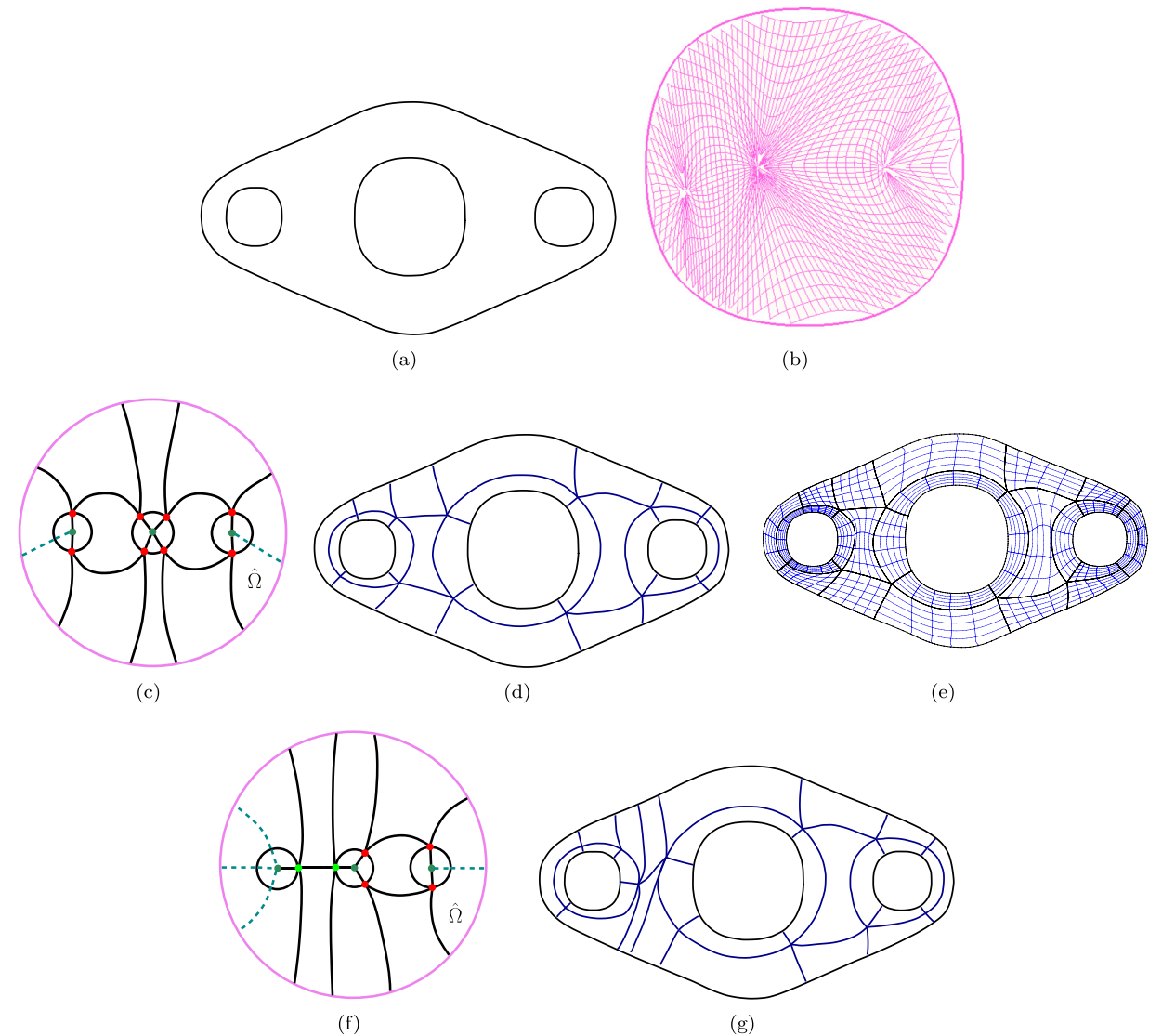


**Fig. 7.** (a) The input domain  $\Omega$  is 4-connected. (b) The behavior of the harmonic mapping  $h$ . The picture exhibits three singular points and no overlappings. (c) A possible template with a segmentation given by EVs of valency 5. (d) The input  $\Omega$  segmented according to template c. (e) A multi-patch parameterization of  $\Omega$ , obtained with THB-splines. (f) A second template for the 4-connected case. (g) The final segmentation of the input  $\Omega$  according to template f.

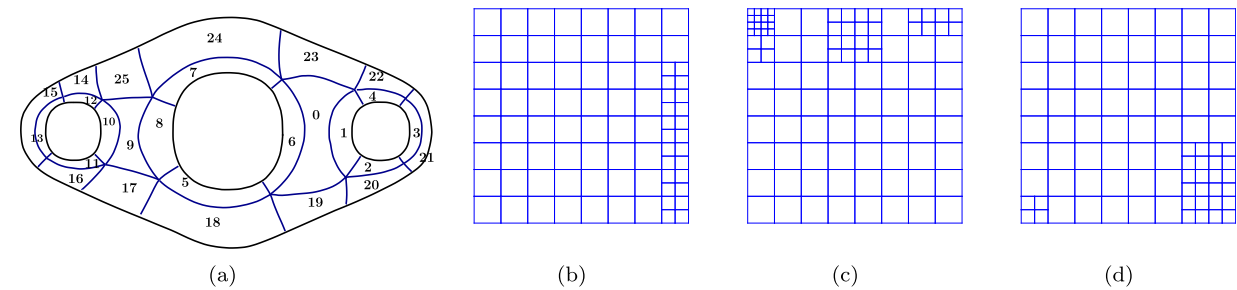


**Fig. 8.** (a) The input domain is segmented according to template in Fig. 7d. The patches are numbered from 0 to 25. The hierarchical meshes are obtained after 6 levels of adaptive refinement. The meshes refer to patch 1 (b), patch 2 (c) and patch 20 (d).

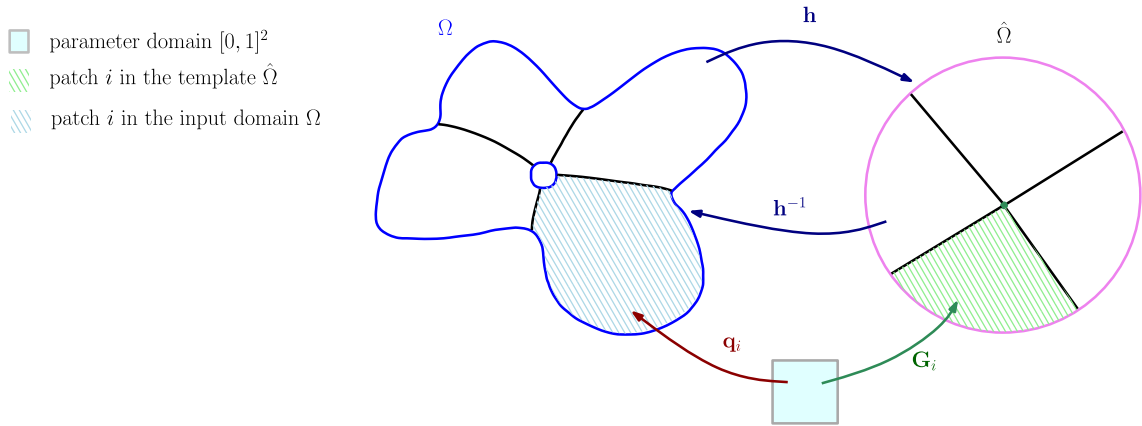


**Fig. 9.** The unit square is given as the parameter domain. The geometric map  $\mathbf{G}_i$  provides a parameterization for each patch of the template  $\hat{\Omega}$ . The solution of the problem (3) gives a mapping  $\mathbf{h}$  defined from  $\Omega$  to  $\hat{\Omega}$ . The desired parameterization  $\mathbf{q}_i$  for each patch  $\Omega^{(i)}$ , is obtained exploiting the combination of the geometric map  $\mathbf{G}_i$  and the inverse mapping  $\mathbf{h}^{-1}$ .

The solution of the minimization problem (17) provides the unknown coefficients  $\mathbf{c}_k^\ell \in \mathbb{R}^2$  for all  $k = 1, \dots, K^\ell$  and all  $\ell = 1 \dots L$ .

We start from an initial tensor-product spline space which is then enlarged by performing adaptive refinement. This procedure is carried out with an error estimator which is based on the computation of the Euclidean distance between the expected value of  $\mathbf{q}_i$  at the parameter points and the effective result provided by the solution of (17).

This methodology is well-known and widely used in the isogeometric-parameterization context. Further details and additional error estimators can be found in [33]. For a general overview about THB-splines and their applications we refer to [17,34,35].

**Remark 1.** In practice, the minimization problem (17) is solved with the additional use of some functional  $\mathcal{Q}(\mathbf{c})$  and a specific weight  $\lambda \in \mathbb{R}$ ,

$$\int_{[0,1]^2} \|\mathbf{q}_i - \mathbf{h}^{-1} \circ \mathbf{G}_i\|^2 + \lambda \mathcal{Q}(\mathbf{c}) \rightarrow \min_{\mathbf{c}} \quad \forall \text{ patch } \Omega^{(i)}, \quad (19)$$

where, to simplify the notation, by  $\mathbf{c} = (\dots, \mathbf{c}_k^\ell, \dots) \in \mathbb{R}^{2,n}$  we denote the matrix of control points  $\mathbf{c}_k^\ell$ . More precisely, we use the following uniformity functional,

$$\mathcal{Q}(\mathbf{c}) = \int_{[0,1]^2} (\|\mathbf{q}_{i,uu}\|^2 + 2\|\mathbf{q}_{i,uv}\|^2 + \|\mathbf{q}_{i,vv}\|^2) du dv. \quad (20)$$

The value for the parameter  $\lambda$  in (19) cannot be determined a-priori. In fact, its value regularizes the effect of the functional  $\mathcal{Q}$  over the resulting parameterization, therefore a good choice for  $\lambda$  is based on a trade-off between accuracy and parameterization quality (further investigation on this topic and applications can be found in [17,33,36] and references cited therein).

## 8. Conclusions

Given a planar multiply-connected domain, we provide a multi-patch parameterization using a THB-spline least square fitting technique. We first describe a segmentation algorithm to split the input  $\Omega$  into patches topologically equivalent to quadrilaterals. The proposed method is based on the construction of templates, i.e. prototypes for segmentations. This construction is not trivial and requires to solve a minimization problem in order to achieve an injective harmonic mapping  $\mathbf{h}$  defined between the input domain  $\Omega$  and the chosen template  $\hat{\Omega}$ . Every template patch  $\hat{\Omega}^{(i)}$  is parametrized using Coons technique. The final multi-patch parameterization of  $\Omega$  is achieved exploiting the combination of the inverse of the harmonic mapping  $\mathbf{h}$ , obtained via projection onto the THB-splines space, and every geometry mapping  $\mathbf{G}_i$  defined for patches  $\hat{\Omega}^{(i)}$ . Our method provides good quality parameterizations, but it is still not a fully automatic procedure. In fact, the selection of the most suitable template should be decided by the user according to the location of the holes in the input  $\Omega$ . Also, the output of some segmentations cannot be predicted a priori: the inverse of the harmonic mapping does not preserve angles between the mapped segmentation curves.

Future work will be devoted to investigate the 3D case, as there are no theoretical guarantees for the existence of a bijective harmonic mapping  $\mathbf{h}$ . Another interesting aspect could be studying the enumeration of all the possible quadrangulations for a given planar shape, in order to achieve a larger or even an exhaustive catalog of prototypes.

## Acknowledgments

This research was supported by EC projects INSIST (GA No. 289361) and the Upper Austria government through the Doctoral Program “Computational Mathematics” at the Johannes Kepler University of Linz. The work was partially supported by the MIUR “Futuro in Ricerca” programme through the project DREAMS (RBFR13FBI3). The corresponding author is member of the INDAM Research group GNCS.

## References

- [1] T.J. Hughes, J.A. Cottrell, Y. Bazilevs, Isogeometric analysis: CAD, finite elements, NURBS, exact geometry and mesh refinement, *Comput. Methods Appl. Mech. Engrg.* 194 (39) (2005) 4135–4195.
- [2] M.K. Agoston, *Computer Graphics and Geometric Modeling*, Vol. 1, Springer, 2005.
- [3] B. Jüttler, M. Kapl, D.-M. Nguyen, Q. Pan, M. Pauley, Isogeometric segmentation: The case of contractible solids without non-convex edges, *Comput. Aided Des.* 57 (2014) 74–90.
- [4] D.-M. Nguyen, M. Pauley, B. Jüttler, Isogeometric segmentation. Part II: On the segmentability of contractible solids with non-convex edges, *Graph. Models* 76 (5) (2014) 426–439.
- [5] B. Strodthoff, B. Jüttler, Layered Reeb graphs for three-dimensional manifolds in boundary representation, *Comput. Graph.* 46 (2015) 186–197.
- [6] G. Farin, D. Hansford, Discrete Coons patches, *Comput. Aided Geom. Design* 16 (7) (1999) 691–700.
- [7] J. Gravesen, A. Evgrafov, D.-M. Nguyen, P. Nørtoft, Planar parametrization in isogeometric analysis, in: *Mathematical Methods for Curves and Surfaces*, Springer, 2014, pp. 189–212.
- [8] K. Hormann, M.S. Floater, Mean value coordinates for arbitrary planar polygons, *ACM Trans. Graph.* 25 (4) (2006) 1424–1441.
- [9] M.S. Floater, K. Hormann, Surface parameterization: a tutorial and survey, in: *Advances in Multiresolution for Geometric Modelling*, Springer, 2005, pp. 157–186.
- [10] K. Hormann, K. Polthier, A. Sheffer, Mesh parameterization: Theory and practice, in: *SIGGRAPH Asia 2008 Course Notes*, Vol. 11, ACM Press, Singapore, 2008, p. v+81.
- [11] J. Xu, F. Chen, J. Deng, Two-dimensional domain decomposition based on skeleton computation for parameterization and isogeometric analysis, *Comput. Methods Appl. Mech. Engrg.* 284 (2015) 541–555.
- [12] F. Buchegger, B. Jüttler, Planar multi-patch domain parameterization via patch adjacency graphs, *Comput. Aided Des.* 82 (2017) 2–12.
- [13] X. Nian, F. Chen, Planar domain parameterization for isogeometric analysis based on teichmüller mapping, *Comput. Methods Appl. Mech. Engrg.* 311 (2016) 41–55.
- [14] G. Xu, M. Li, B. Mourrain, T. Rabczuk, J. Xu, S.P. Bordas, Constructing iga-suitable planar parameterization from complex cad boundary by domain partition and global/local optimization, *Comput. Methods Appl. Mech. Engrg.* 328 (2018) 175–200.
- [15] Y. Zhang, W. Wang, T.J. Hughes, Conformal solid T-spline construction from boundary T-spline representations, *Comput. Mech.* 51 (6) (2013) 1051–1059.
- [16] H. Speleers, C. Manni, Optimizing domain parameterization in isogeometric analysis based on powell–sabin splines, *J. Comput. Appl. Math.* 289 (2015) 68–86.
- [17] A. Falini, J. Špeh, B. Jüttler, Planar domain parameterization with THB-splines, *Comput. Aided Geom. Design* 35 (2015) 95–108.
- [18] P. Duren, W. Hengartner, Harmonic mappings of multiply connected domains, *Pacific J. Math.* 180 (1997) 201–220.
- [19] L. Gaul, M. Kögl, M. Wagner, *Boundary Element Methods for Engineers and Scientists*, in: *Engineering Online Library*, Springer, 2003.
- [20] S. Sauter, C. Schwab, *Boundary Element Methods*, Springer, Berlin, 2011.
- [21] R. Simpson, S. Bordas, J. Trevelyan, T. Rabczuk, A two-dimensional isogeometric boundary element method for elastostatic analysis, *Comput. Methods Appl. Mech. Engrg.* 209 (2012) 87–100.
- [22] M. Guiggiani, P. Casalini, Direct computation of Cauchy principal value integrals in advanced boundary elements, *Internat. J. Numer. Methods Engrg.* 24 (9) (1987) 1711–1720.
- [23] G. Monegato, Numerical evaluation of hypersingular integrals, *J. Comput. Appl. Math.* 50 (1) (1994) 9–31.
- [24] A. Aimi, F. Calabrò, M. Diligenti, M. Sampoli, G. Sangalli, A. Sestini, Efficient assembly based on b-spline tailored quadrature rules for the iga-sgbem, *Comput. Methods Appl. Mech. Engrg.* 331 (2018) 327–342.
- [25] F. Calabrò, A. Falini, M.L. Sampoli, A. Sestini, Efficient quadrature rules based on spline quasi-interpolation for application to iga-bems, *J. Comput. Appl. Math.* (2018).
- [26] A.R. Conn, K. Scheinberg, P.L. Toint, Recent progress in unconstrained nonlinear optimization without derivatives, *Math. Program.* 79 (1–3) (1997) 397–414.
- [27] S. Lucidi, M. Sciandrone, On the global convergence of derivative-free methods for unconstrained optimization, *SIAM J. Optim.* 13 (1) (2002) 97–116.
- [28] E. Rank, M. Ruess, S. Kollmannsberger, D. Schillinger, A. Düster, Geometric modeling, isogeometric analysis and the finite cell method, *Comput. Methods Appl. Mech. Engrg.* 249 (2012) 104–115.
- [29] D. Schillinger, L. Dede, M.A. Scott, J.A. Evans, M.J. Borden, E. Rank, T.J. Hughes, An isogeometric design-through-analysis methodology based on adaptive hierarchical refinement of NURBS, immersed boundary methods, and T-spline CAD surfaces, *Comput. Methods Appl. Mech. Engrg.* 249 (2012) 116–150.
- [30] C.-H. Peng, M. Bartoň, C. Jiang, P. Wonka, Exploring quadrangulations, *ACM Trans. Graph.* 33 (1) (2014) 12.
- [31] L. Piegl, W. Tiller, *The NURBS Book*, Springer Science & Business Media, 2012.
- [32] A. Falini, *Isogeometric Segmentation of Planar Domains using Harmonic Mappings* (Ph.D. thesis), Johannes Kepler University, Linz, 2016. <http://epub.jku.at/obvuihs/download/pdf/1302456?originalFilename=true>.
- [33] G. Kiss, C. Giannelli, U. Zore, B. Jüttler, D. Großmann, J. Barner, Adaptive CAD model (re-) construction with THB-splines, *Graph. Models* 76 (5) (2014) 273–288.
- [34] C. Giannelli, B. Jüttler, S.K. Kleiss, A. Mantzaflaris, B. Simeon, J. Špeh, THB-splines: An effective mathematical technology for adaptive refinement in geometric design and isogeometric analysis, *Comput. Methods Appl. Mech. Engrg.* 299 (2016) 337–365.
- [35] C. Giannelli, B. Jüttler, H. Speleers, THB-splines: The truncated basis for hierarchical splines, *Comput. Aided Geom. Design* 29 (7) (2012) 485–498.
- [36] V. Weiss, L. Andor, G. Renner, T. Várady, Advanced surface fitting techniques, *Comput. Aided Geom. Design* 19 (1) (2002) 19–42.